Geomechanics and Engineering, *Vol. 23, No. 5 (2020) 405-418*
DOI: https://doi.org/10.12989/gae.2020.23.5.405

A simplified combined analytical method for evaluating the effect of deep surface excavations on the shield metro tunnels

Bo Liu*[1], Zhiwei Yu[1], Yanhui Han[2], Zhiliu Wang[3], Shuo Yang[1] and Heng Liu[1]

[1]*School of Mechanics & Civil Engineering, China University of Mining and Technology, Beijing No.11, Xueyuan Road, Beijing, China*
[2]*Department of Civil, Environmental and Geo-Engineering, University of Minnesota, SE Walnut Street, Minnesota, U.S.A.*
[3]*School of Civil Engineering and Architecture, Zhongyuan University of Technology, No.41 Zhongyuan Middle Road, Zhengzhou, Henan Province, China*

(Received August 12, 2020, Revised October 26, 2020, Accepted November 16, 2020)

Abstract. Deep excavation may have impact on the adjacent tunnels. It is obvious that the excavation will adversely affect and even damage the existing tunnels if the induced deformation exceeds the capacity of tunnel structures. It hence creates a high necessity to predict tunnel displacement induced by nearby excavation to ensure the safety of tunnel. In this paper, a simplified method to evaluate the heave of the underlying tunnel induced by adjacent excavation is presented and verified by field measurement results. In the proposed model, the tunnel is represented by a series of short beams connected by tensile springs, compressional springs and shear springs, so that the rotational effect and shearing effect of the joints between lining rings can be captured. The proposed method is compared with the previous modelling methods (e.g., Euler-Bernoulli beam, a series of short beams connected only by shear springs) based on a field measured longitudinal deformation of subway tunnels. Results of these case studies show a reasonable agreement between the predictions and observations.

Keywords: deep surface excavation; tunnel heave; rotational effect; shearing effect

1. Introduction

In China's urban construction, more and more new deep foundation pit projects will be constructed above or on the side of existing underground structures such as subway tunnels. The environmental impact of a deep foundation pit during its construction has become one of the most important factors that designers must consider. For example, the excavation of a foundation pit will lead to unconfined displacement of the surrounding soil, which interacts with the subway tunnel, resulting in displacement and stress changes around the tunnel.

This problem has attracted tremendous attention internationally and lots of researches have been carried out. Many physical model tests have been performed to understand the mechanisms of excavation-tunnel interactions (Ng *et al.* 2013, Marshall *et al.* 2010, Zheng *et al.* 2017, Nam *et al.* 2020). Numerical simulation is another often-used effective research method in the investigation of this problem (Shi *et al.* 2015, Huang *et al.* 2013, Bousbia and Messast 2015, Do *et al.* 2018, Liu *et al.* 2011, Nooraddin and Mohammad 2016, Zhang *et al.* 2016, Zhang and Huang 2014). The physical tests are usually very demanding on the time and resources, and their accuracy is influenced by many factors such as instrument precision, personnel operation, etc. The accuracy of simulation results is dependent on the reliability and accuracy of input parameters.

Analytical solution approach is also widely adopted in the deep excavation-soil-tunnel interaction analysis (Zhang *et al.* 2013, Wang *et al.* 2019). This method has much lower computational cost and can make rapid predictions on the behaviors of existing tunnels. Zhang *et al.* (2013) assumed the existing shield tunnel as an elastic beam and evaluated the tunnel deformation induced by an adjacent excavation based on Boussinesq's and Mindlin's solutions, respectively. In the analysis of the interaction between the excavation and the tunnel, the existing tunnel was often simplified as Euler-Bernoulli beam in some existing works (Basile 2014, Liang *et al.* 2018, Vorster *et al.* 2005, Tanahashi 2004, Zhang *et al.* 2015, Talmon and Bezuijen 2012, Liu *et al.* 2019). Liang *et al.* (2018) adopted the Euler-Bernoulli beam model to study the responses of the existing tunnel induced by unloading of deep excavation, and verified their analytical solutions by the finite element method analysis and two published filed measurements. One major drawback of these analytical solutions is that, the existing tunnel was represented by an elastic beam or Euler-Bernoulli beam, which can consider the bending deformation but have to ignore the shear deformation. Considering that Timoshenko beam model (Wu *et al.* 2015, Li *et al.* 2016, Liang *et al.* 2017, Zhang *et al.* 2019) can capture the shear deformation of the shield tunnel, Liang *et al.* (2017) treated the existing tunnel as Timoshenko beam resting on Pasternak foundation and derived a theoretical solution of the shield tunnel subjected to the excavation of deep foundation pit through a two-stage method. Besides

*Corresponding author, Professor
E-mail: liub@cumtb.edu.cn

ISSN: 2005-307X (Print), 2092-6219 (Online)

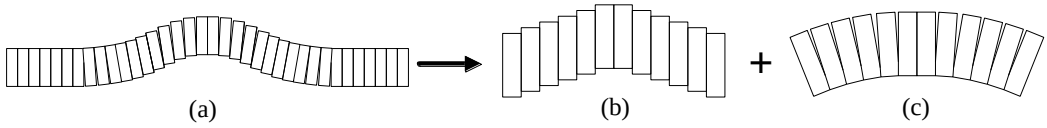

(a) Tunnel deformation mode (b) Shearing dislocation mode (c) Bending mode

Fig. 1 Diagram of tunnel deformation mode

Timoshenko beam, an elastic short beam connected by shear springs can also capture the shearing effect of the joints between the segmental rings, so it was also used to represent the existing tunnel (Wei *et al.* 2018, 2019).

As reviewed above, in most previous work the existing tunnel was modeled as an infinite beam and modeled by Euler-Bernoulli beam, Timoshenko beam, or short beams connected by shear springs. These works can consider the overall bending of the beam or shearing effect of the bolts, but they cannot explain the opening between the tunnel lining rings. In reality, the lining of a shield tunnel is composed of precast reinforced concrete segments connected by steel bolts (Cheng *et al.* 2017). However, the bolt joints were overlooked in most existing models.

To fill this gap, in this work the existing shield tunnel is extended as short beams connected by shear springs, tensile springs and compressive springs. This model is capable of capturing both shearing and the rotational effects of the joints between the lining rings, thus allowing a complete investigation of the deformation of an existing shield tunnel during the adjacent deep excavation.

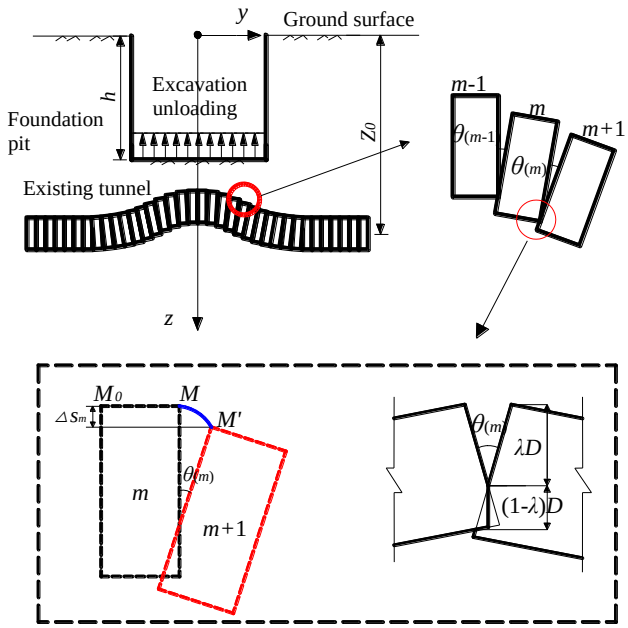

Fig. 2 Local deformation mode of tunnel

2. Modelling a deep surface excavation over a shield tunnel

Wu *et al.* (2015), Liang *et al.* (2017) and Liu *et al.* (2020) all indicated that the longitudinal deformation of the tunnel can be decomposed into two different modes: the shear dislocation mode between the lining rings and bending mode, as shown in Fig. 1. However, due to the existence of circumferential joints between segmental rings, the deformation characteristics of shield tunnel is obviously different from that of continuous beam structure. The previous beam models cannot fully describe the structural deformation characteristics of shield tunnels.

In order to analyze the response of the existing tunnel under adjacent excavation, a deformation model of tunnel structure is proposed in this work, as shown in Fig. 2. The shield tunnel is represented by a series of short beams connected by shearing springs, tensile springs and compressive springs. The model considers not only the bending of the beam, but also the shear and rotation effects between the lining rings. The assumptions made in the development of our new model are as follows:

(1) Assuming that the soil is an isotropic, homogeneous and continuous semi-infinite elastic material and the tunnel is always connected with the stratum without detachment. The time-dependent behaviors of the existing deformation of the tunnel and the soil-tunnel interaction, such as consolidation and creep, are not considered;

(2) The deformation at the joints is mainly caused by the deformation of the bolts and the concrete compression deformation of the joint surface. When the lining rings is opened, the compressional contact area and the separational area of the surface between the tunnel lining rings are flat planes, such that the assumption of flat sections is satisfied. As the opening between the lining rings is small, it is assumed that the force of bolt joint varies linearly;

(3) The influence of the embossed groove and the water-swellable rubber filler is negligible.

The deformation of tunnel structure includes not only the dislocation between adjacent lining rings but also the rotation of lining rings. As shown in Fig. 2, taking three lining rings, numbered as ‘m-1’, ‘m’, ‘m+1’ respectively, as an example, the relative displacement between the ring ‘m’ and the ring ‘m+1’ is ΔS_m and the angle between ring ‘m’ and the ring ‘m+1’ is $\theta_{(m)}$.

Liu *et al.* (2020) regarded the tunnel as a series of short beams connected by springs and calculated its deformation. While the bending deformation was approximately regarded as the relative displacement between the lining rings in the caculation. Wei *et al.* (2018) and Wei *et al.* (2019) proposed a rotation coefficient α to describe the relationship between the bending deformation (ΔS_2) and relative displacement between the lining rings, namely $\Delta S_2 = \alpha \Delta S$. It should be pointed out that α is a fixed value (α= 0.1), which means that the displacement caused by shearing dislocation is always 9 times the displacement of bending deformation. Obviously, this linear relationship is not consistent with reality. It can be seen that the above two methods both use

approximation, and cannot consistently describe the deformation of the tunnel. In fact, the bending deformation between two adjacent points of a curve has a great relationship with the bending degree. To fill this gap, this work solves the bending deformation between lining rings according to the curve bending degree and geometric relationship. The expression is:

$$\widehat{MM'} = \delta\sqrt{1+S'^2(x)} \tag{1}$$

where $\widehat{MM'}$ is the bending deformation between two adjacent lining rings; δ is the width of the lining ring; $S(x)$ is the longitudinal displacement of the tunnel.

3. Analysis method

3.1 Unloading stress caused by excavation

This study considers the general situation of tunnels parallel to the rectangular foundation pit boundary. Fig. 3 shows the relative position of the existing tunnel and the excavation. The length of the foundation pit is L, the width is B, and the excavation depth is h. The existing tunnel is parallel to the x-axis, the distance between the tunnel axis and the excavation x-axis is d and the outer diameter of the tunnel is D. In this study, the soil is assumed to be homogeneous (layered soil can be converted into homogeneous soil according to Poulos and Davis (1980) method), the soil weight is γ, the soil Poisson's ratio is μ. The rectangle uniform load calculated by γh is applied on the excavation bottom. The unloading stress of the existing tunnel caused by the uniformly distributed load is a typical semi-infinite space problem. Therefore, the Mindlin's solution (Mindlin 1936) can be used to calculate the unloading stress caused by excavation of a foundation pit. According to the Mindlin's solution, the unloading stress $\sigma(x)$ caused by excavation at the level of the tunnel is obtained:

According to Mindlin's solution, the additional stress induced by a concentrated force at depth of z_0 can be obtained:

$$\sigma_z = \frac{Q}{8\pi(1-\mu)}\left[\frac{(1-2\mu)(z_0-h)}{T_1^3}+\frac{3(z_0-h)^3}{T_1^5}-\frac{(1-2\mu)(z_0-h)}{T_2^3}+\frac{3(3-4\mu)z_0(z_0+h)^2-3h(z_0+h)(5z_0-h)}{T_2^5}+\frac{30z_0h(z_0+h)^3}{T_2^7}\right] \tag{2}$$

where Q is the concentrated force in the soil.

From Eq. (2), it can be seen that at a certain point (x, y, z_0) on the tunnel axis level, the vertical additional stress σ_z caused by the concentrated force pdξdη at a point (ξ, η) in the uniform load is:

$$\sigma_z = \frac{P}{8\pi(1-\mu)}\left\{(1-2\mu)(z_0-h)\int_A\int\frac{d\xi d\eta}{T_1^3}+3(z_0-h)^3\int_A\int\frac{d\xi d\eta}{T_1^5}-(1-2\mu)(z_0-h)\int_A\int\frac{d\xi d\eta}{T_2^3}+3(3-4\mu)z_0(z_0+h)^2-3h(z_0+h)(5z_0-h)\int_A\int\frac{d\xi d\eta}{T_2^5}+30z_0h(z_0+h)^3\int_A\int\frac{d\xi d\eta}{T_2^7}\right\} \tag{3}$$

The bottom area of the excavation is $L\times B$, and the uniform load is γh. Combining Eqs. (2) and (3), we have:

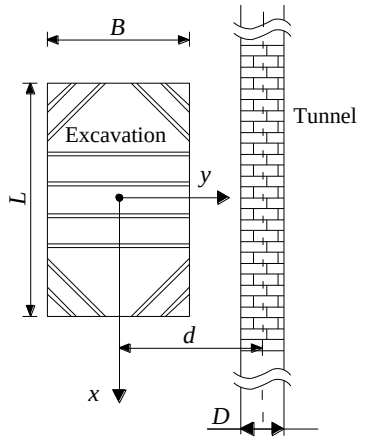

Fig. 3 Diagram of the tunnel and the excavation

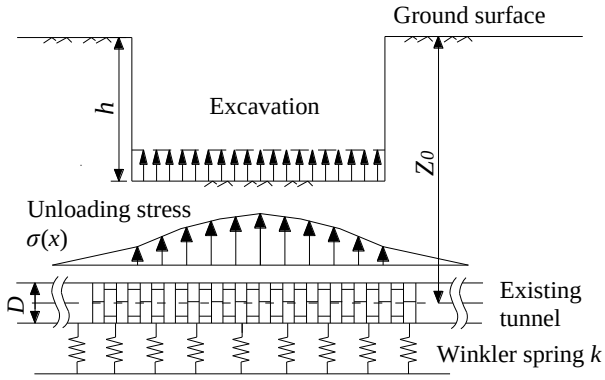

Fig. 4 Calculation model

$$\sigma(x) = -\frac{\gamma h}{8\pi(1-\mu)}\int_{-B/2}^{B/2}\int_{-L/2}^{L/2}\left[\frac{(1-2\mu)(z_0-h)}{T_1^3}-\frac{(1-2\mu)(z_0-h)}{T_2^3}+\frac{3(z_0-h)^3}{T_1^5}+\frac{3(3-4\mu)z_0(z_0+h)^2-3h(z_0+h)(5z_0-h)}{T_2^5}+\frac{30z_0h(z_0+h)^3}{T_2^7}\right]d\xi d\eta \tag{4}$$

where

$T_1=\sqrt{(x-\xi)^2+(d-\eta)^2+(z_0-h)^2}$, $T_2=\sqrt{(x-\xi)^2+(d-\eta)^2+(z_0+h)^2}$;

z_0 is the buried depth of the tunnel (m).

3.2 Tunnel deformation due to excavation

The calculation model the existing tunnel caused by the excavation is shown in Fig. 4. The tunnel is modeled as a series of short beams connected by shear springs, tensile springs and compressive springs on Winkler foundation (Winkler 1867). As shown in Fig. 4, the unloading stress due to the excavation causes the existing tunnel to deform. The final deformation of the existing tunnel is determined by the unloading stress, foundation reaction and the force between the lining rings. In this work, the energy method is used to solve the deformation of the existing tunnel. First, an appropriate deformation function is assumed, and the energy variation equation is established by summing up the work done by each force and solving the deformation function. Wei *et al.* (2018) used the energy method to solve the deformation of pipes and tunnels.

Fig. 5 shows the force analysis for an individual lining

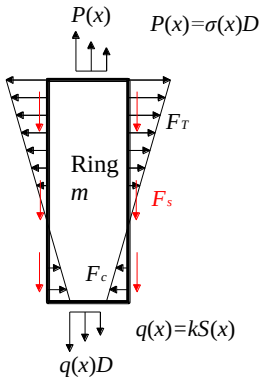

Fig. 5 Force analysis diagram of an individual lining ring

ring. In the vertical direction this lining ring is subjected to an upward stress $P(x)$, a downward subgrade reaction stress $(q(x)D)$ and an inter-ring shear stress F_s. In the horizontal direction, it is subjected to an inter-ring tensile stress F_T and compressive stress F_c. $\sigma(x)$ and $q(x)$ are the vertical unloading stress caused by excavation and reaction pressure, respectively; D is the outer diameter of the tunnel. Based on the free body diagram analysis for an individual ring of the tunnel in Fig. 5, the total potential energy of the existing shield tunnel caused by excavation consists of the following five parts:

(1) Work done by unloading stress $\sigma(x)$ caused by excavation:

$$W_\sigma = \sum_{\mathrm{m}=-N}^{N-1} \int_{m\delta}^{(m+1)\delta} S(x)P(x)dx = \int_{-N\delta}^{N\delta} S(x)\sigma(x)Ddx \tag{5}$$

(2) Work done to overcome the resistance of the formation $q(x)$:

$$W_q = -\sum_{m=-N}^{N-1} \int_{m\delta}^{(m+1)\delta} \frac{1}{2}kDS^2(x)dx = -\int_{-N\delta}^{N\delta} \frac{1}{2}kDS^2(x)dx \tag{6}$$

(3) Work done to overcome the shear force between the rings F_s:

$$W_s = -\sum_{m=-N}^{N-1} \frac{1}{2}k_s\left[S((m+1)\delta) - S(m\delta)\right]^2 \tag{7}$$

(4) Work done by tensile stress between rings F_T (note, it is assumed that the force of joint varies linearly):

$$W_T = -\sum_{m=-N}^{N-1}\left[\int_0^{\lambda D} \frac{k_T}{\lambda D}\theta_m r \frac{\theta_m r}{2}dr\right] = -\sum_{m=-N}^{N-1} \frac{\lambda^2 D^2 k_T \theta_m{}^2}{6} \tag{8}$$

(5) Work done by compressional stress between rings F_c:

$$W_c = -\sum_{m=-N}^{N-1}\left[\int_0^{(1-\lambda)D} \frac{k_c}{(1-\lambda)D}\theta_m r \frac{\theta_m r}{2}dr\right] = -\sum_{m=-N}^{N-1} \frac{(1-\lambda)^2 D^2 k_c \theta_m{}^2}{6} \tag{9}$$

where k is coefficient of subgrade modulus; k_s is the inter-ring shear stiffness (N/m); k_T is the inter-ring tensile stiffness (N/m); k_c is the inter-ring compressive stiffness (N/m); λ is the proportion coefficient of the tension area of the lining ring; 2N is the number of existing tunnel lining rings affected by excavation.

According to the geometric relationship in Fig. 2, the equation on the angle θ_m can be obtained:

$$\theta_m = \frac{MM'}{\lambda D} \tag{10}$$

Since the bending moments of the upper and lower sides of the lining ring are the same, the bending moment equilibrium gives:

$$\int_0^{\lambda D} \frac{k_T r^2 \theta_m}{\lambda D}dr = \int_0^{(1-\lambda)D} \frac{k_c r^2 \theta_m}{(1-\lambda)D}dr \tag{11}$$

According to Eq. (1) and Eq. (10), Eqs. (8)-(9) can be converted into:

$$W_T = -\sum_{m=-N}^{N-1} \frac{\lambda^2 D^2 k_T \theta_m{}^2}{6} = -\sum_{m=-N}^{N-1} \frac{k_T \delta^2}{6}\left[1 + S'^2(m\delta)\right] \tag{12}$$

$$W_c = -\sum_{m=-N}^{N-1} \frac{(1\text{-}\lambda)^2 D^2 k_c \theta_m{}^2}{6} = -\sum_{m=-N}^{N-1} \frac{(1\text{-}\lambda)^2 k_c \delta^2}{6\lambda^2}\left[1 + S'^2(m\delta)\right] \tag{13}$$

Therefore, the total potential energy of the shield tunnel caused by excavation is:

$$E = W_\sigma + W_q + W_s + W_T + W_c \tag{14}$$

The principle of energy variation method assumes a suitable displacement function representing the basic deformation shape of the shield tunnel. Han *et al.* (2012) respectively collected dozens of sets of existing tunnel deformation data caused by adjacent excavation in London and Beijing, and concluded that the tunnel deformation conforms to normal distribution. In addition, the energy variation method was used to solve the deformation equation of the tunnel and verifies the accuracy of this method through practical engineering in the literature (Wei *et al.* 2018, Liu *et al.* 2014, Wei *et al.* 2019). In this work, the tunnel displacement function is assumed to follow normal distribution with Fourier series expansion (Liu *et al.* 2014):

$$S(x) = \sum_{n=0}^{\infty} a_n \cos\frac{n\pi x}{N\delta} = \boldsymbol{T}_n(x)\boldsymbol{A} \tag{15}$$

$$\boldsymbol{T}_n(x) = \left\{1, \cos\frac{\pi x}{N\delta}, \cos\frac{2\pi x}{N\delta}, \cdots, \cos\frac{n\pi x}{N\delta}\right\} \tag{16}$$

$$\boldsymbol{A} = \left\{a_1, a_2, a_3, \cdots, a_n\right\}^{\mathrm{T}} \tag{17}$$

where $\boldsymbol{A}$ is the undetermined coefficient matrix of the displacement function; n is the expansion order of the Fourier series.

Based on the energy variation method, the total potential energy E is taken as the extreme value of each undetermined coefficient, i.e.,

$$\frac{\partial E}{\partial \xi_i} = 0\ (\xi_i = a_1, a_2, a_3, \cdots, a_n) \tag{18}$$

where ξ_i is an individual element in matrix $\boldsymbol{A}$, which is the coefficient of the tunnel vertical displacement's polynomial function.

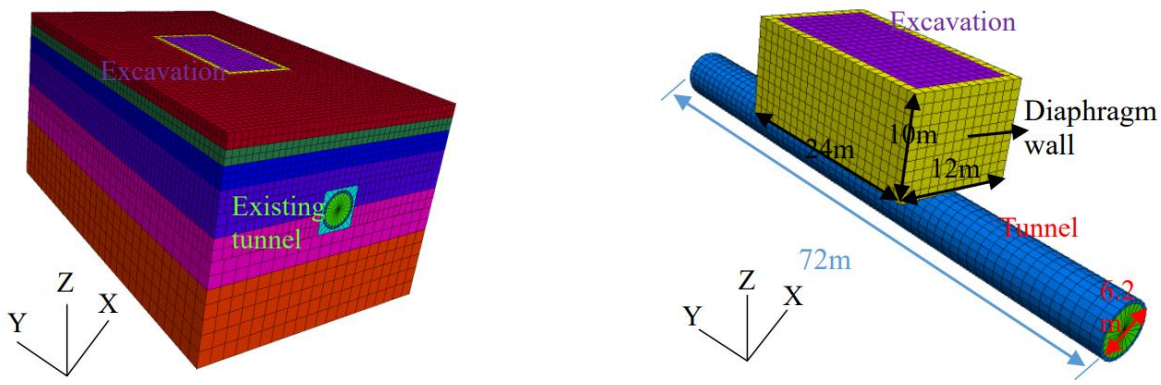

(a) Geometric model (b) Details of the tunnel and excavation

Fig. 6 3D finite difference model

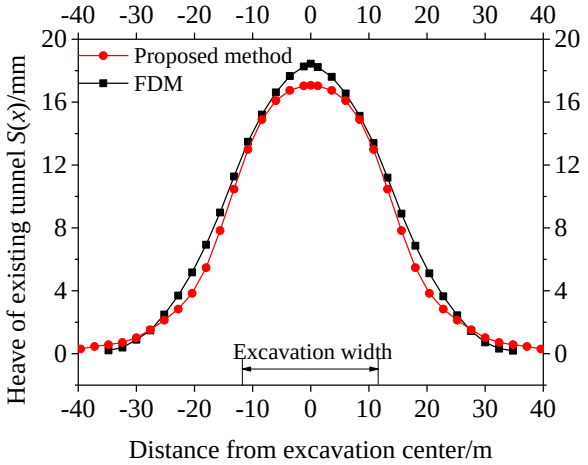

Fig. 7 Tunnel heave with different methods

Solving the Eq. (18) gives the governing equation:

$$\left\{\int_{-N\delta}^{N\delta} kDT_n(x)\frac{\partial S(x)}{\partial \xi_i}dx+\sum_{m=-N}^{N-1}k_s\left\{T_n\left[(m-1)\delta\right]-T_n(m\delta)\right\}\cdot\frac{\partial\{S\left[(m-1)\delta\right]-S(m\delta)\}}{\partial \xi_i}+\sum_{m=-N}^{N-1}\frac{2k_T\delta^2}{3}T_n'(m\delta)\frac{\partial S'(m\delta)}{\partial \xi_i}\right\}\cdot A=\int_{-N\delta}^{N\delta}P(x)\{T_n(x)\}^{\mathrm{T}}dx \tag{19}$$

Eq. (19) can also be expressed in the form of a matrix:

$$(\boldsymbol{K}_k+\boldsymbol{K}_s+\boldsymbol{K}_r)\boldsymbol{A}=\boldsymbol{P}^{\mathrm{T}} \tag{20}$$

$$\boldsymbol{K}_k=kDN\delta\begin{bmatrix}2 & & & \\ & 1 & & \\ & & \ddots & \\ & & & 1\end{bmatrix} \tag{21}$$

$$\boldsymbol{K}_s=\sum_{m=-N}^{N-1}k_s\left\{\boldsymbol{T}_n^{\mathrm{T}}\left[(m-1)\delta\right]-\boldsymbol{T}_n^{\mathrm{T}}(m\delta)\right\}\left\{\boldsymbol{T}_n\left[(m-1)\delta\right]-\boldsymbol{T}_n(m\delta)\right\} \tag{22}$$

$$\boldsymbol{K}_r=\sum_{m=-N}^{N-1}\frac{2k_T\delta^2}{3}\cdot\boldsymbol{T}_n'^{\mathrm{T}}(m\delta)\cdot\boldsymbol{T}_n'(m\delta) \tag{23}$$

$$\boldsymbol{P}^{\mathrm{T}}=\int_{-N\delta}^{N\delta}P(x)\{\boldsymbol{T}_n(x)\}^{\mathrm{T}}dx \tag{24}$$

where $\boldsymbol{K}_k$ is the soil stiffness matrix; $\boldsymbol{K}_s$ is the tunnel inter-ring shear stiffness matrix; $\boldsymbol{K}_r$ is the tunnel inter-ring rotational stiffness matrix; and $\boldsymbol{P}^T$ is the interaction effect between the free soil displacement and the tunnel lining ring.

The above formula is numerically solved by Matlab programming. From Eq. (20), the matrix $\boldsymbol{A}$ of the undetermined coefficients can be obtained. Taking the 10th order stiffness matrix $\boldsymbol{K}_k$, $\boldsymbol{K}_s$ and $\boldsymbol{K}_r$ can satisfy the calculation accuracy.

According to the tunnel deformation and the shear stiffness between rings, the relative displacement ΔS and shear force Q between rings can be obtained. The expression is as follows:

$$\Delta S=S[(m+1)\delta]-S(m\delta) \tag{25a}$$

$$Q=\left\{S[(m+1)\delta]-S(m\delta)\right\}\cdot k_s \tag{25b}$$

The flow chart of calculation procedure of the proposed method is shown in Fig. 19.

4. Validation

4.1 Comparison with 3D numerical analysis

A three-dimensional finite difference model (FDM) was established to study the tunnel deformation caused by

excavation as shown in Fig. 6. The length, width, and depth of the excavation are 24 m, 12 m and 10 m respectively; four underground continuous walls are set outside the foundation pit to support lateral earth pressure. The outer diameter of the tunnel is 6.2 m, the lining ring width is 1.2 m, and the buried depth is 15 m. Since the focus is to analyze the longitudinal deformation of the existing tunnel rather than the deformation of the lining ring, the lining ring is simplified as a whole ring instead of a segmented-ring. Cable structure element is used to simulate the bolt between lining rings. According to the actual project, the bolt length is 0.4 m, and there are 17 bolts between each two rings. The cable structure element has an elastic modulus of 2.06 GPa. According to the Appendix, the shear stiffness k_s=2.47×10^{6}kN/m, the tensile stiffness k_T=1.73×10^5 kN/m and the compressive stiffness k_c=1.79×10^8 kN/m. The elastic modulus of the soil is 10 MPa, the Poisson's ratio is 0.3, and the soil unit weight is 18 kN/m^3.

Fig. 7 shows the comparison between the tunnel heave calculated by FDM and our new method. The calculation results our new method are in good agreement with the FDM calculation results, although the maximum value is slightly smaller. This may be because the excavation of the foundation pit during the FDM calculation may cause the local stiffness of the tunnel ground to be locally reduced, which cannot be further considered in our new method.

4.2 Comparison with beam methods from literature

Liang *et al.* (2017) and Huang *et al.* (2013) reported an underground passage in Shanghai. The underground passage was constructed by cut-and-cover method, and perpendicular to an existing tunnel. The length, width and depth of the excavation are 50 m, 10 m and 11 m, the depth of the center of the tunnel is 22 m, and the clearance between excavation bottom and tunnel crown is about 5.5 m. The outer diameter of the tunnel is 11 m, and the length of each segmental lining is 1 m, as shown in Fig.8. In order to protect the shield tunnel, the excavation of the foundation pit is divided into 3 parts. Detailed information can be found in Huang *et al.* (2013), where they conducted a series of three-dimensional finite element simulations to analyze the heave of the existing tunnel. Liang *et al.* (2017) calculated the heave of the existing tunnel based on the Timoshenko beam method and Euler-Bernoulli beam method, respectively. In their study the bending stiffness of the tunnel is 3.99×10^5 MN•m^2, and the shear stiffness is 3.38×10^3 MN/m. The soil elastic modulus is taken as 15 MPa, and the average Poisson's ratio is taken as 0.3. According to the Appendix, the tensile stiffness and the compressive stiffness are taken as 6.46×10^4 kN/m and 6.05×10^8 kN/m.

The displacement of the existing tunnel during excavation is predicted by our new method, and the results are compared with the results of finite element simulation and the beam methods as shown in Fig. 9. The maximum heave of the tunnel using our new method, Timoshenko beam method and Euler-Bernoulli beam method is 20.4 mm, 22.5 mm and 21.0 mm respectively. Compared with Euler Bernoulli beam method, Timoshenko beam method takes into account the shear effect, subsequently the

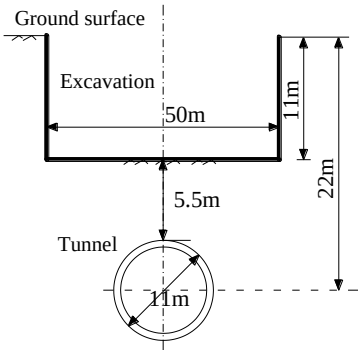

Fig. 8 Sectional view of excavation and tunnel

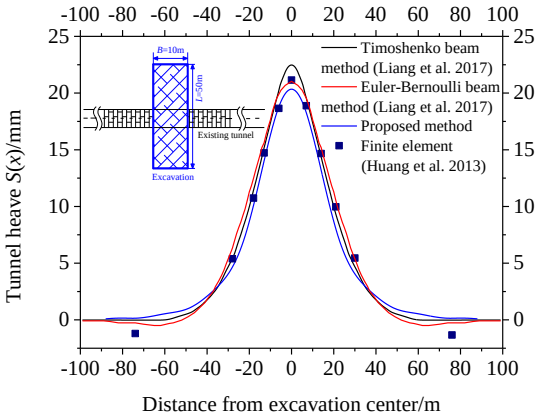

Fig. 8 Sectional view of excavation and tunnel

calculation result of tunnel heave is slightly larger. In comparison, in our new method the shield tunnel is regarded as a series of short beams connected by springs, which considers the shear dislocation between the lining rings and the rotation effect of the lining rings. As a result, the calculated value is smaller than two beam methods. When encountering the same unloading energy, the short beam structures have not only the overall bending and joint dislocation, but also the rotation of lining ring; while the beam only has the first two deformation components. It should be noted that the difference between the maximum heaves given by the three calculation methods and the finite element model (i.e., 21.1 mm) is relatively very small. General speaking, all three methods can be used to predict the deformation of the existing tunnel under the excavation of the foundation pit.

Fig. 10 shows the shear force and tunnel deformation calculated by Timoshenko beam method, Euler-Bernoulli beam method and the new method in this paper. Fig. 10a shows the longitudinal shear force distribution of the tunnel. It can be seen that the shear force is symmetric about the origin. Comparing the three methods, the calculation value of our new method is larger than those of two beam methods, and the influence range of the shear force calculated by our new method is also larger. This is because two beam methods do not take into account the bolt connection between the lining rings. Even though the Timoshenko beam method considers the shear effect between the plane sections, it seems to be insufficient. In our new method, a series of short beams connected by

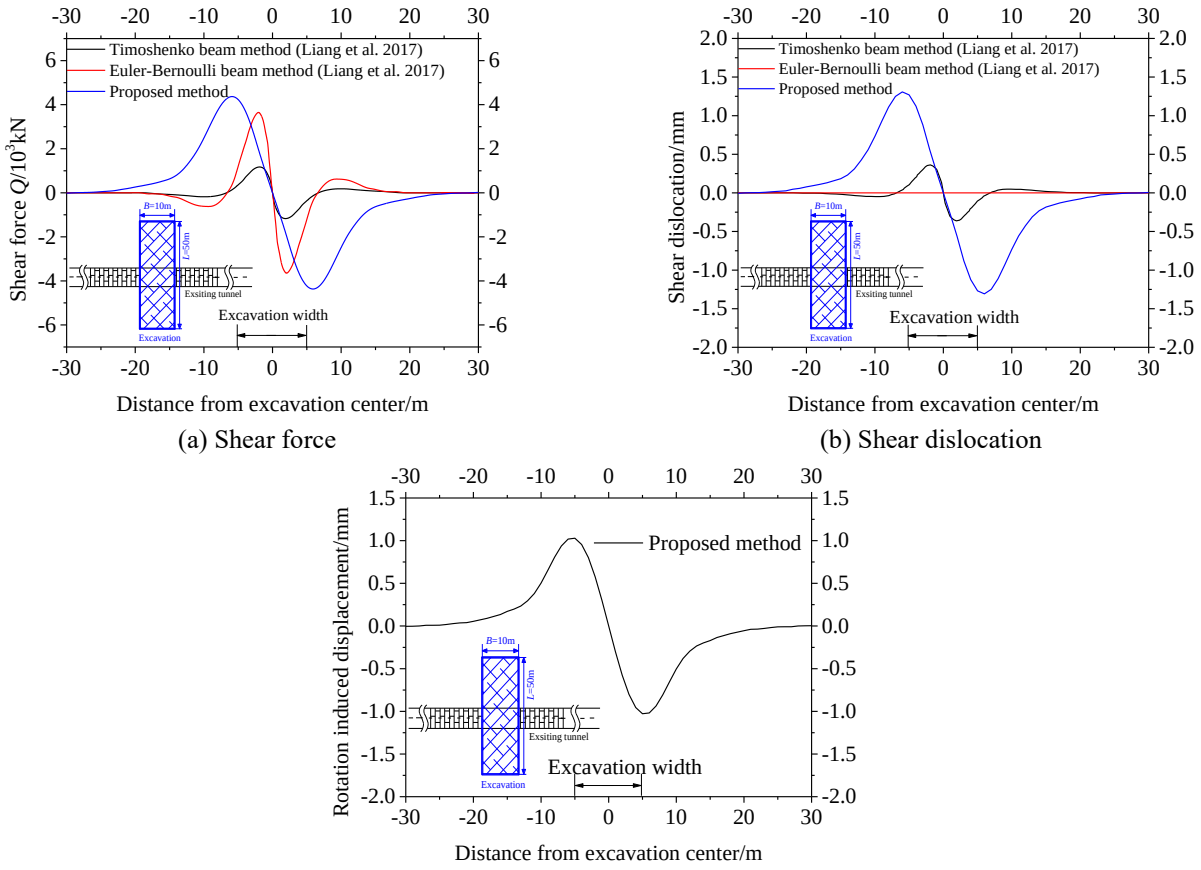

(a) Shear force (b) Shear dislocation

(c) Rotation induced displacement

Fig. 10 Shear force and relative displacement distribution

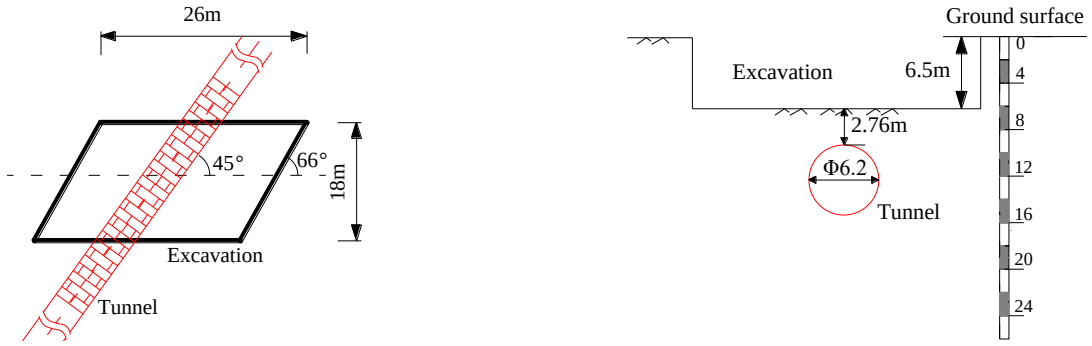

(a) Plan view (b) Sectional view

Fig.11 Relationship between the excavation and the tunnel

springs can directly consider the shear dislocation and stress between the lining rings. As described by Liang *et al.* (2017), the maximum shear force is located on both sides of the foundation pit, so it is necessary to pay a close attention to the integrity of the tunnel lining structure at these locations. Fig. 10(b) shows the dislocations between adjacent segment linings along the longitudinal direction of the tunnel. Similarly, the calculation result of our new method is the largest. Because the Euler-Bernoulli beam method cannot take into account the dislocation between the lining rings, the shear dislocation between the rings is 0. Although the Timoshenko beam method takes into account the shear effect between the plane sections, the shear dislocation between the lining rings is still underestimated. Fig. 10(c) shows the distribution of rotation induced displacement of the lining rings. The maximum value of the deformation appears on both sides of the foundation pit instead of the middle of the foundation pit. This is consistent with the conclusion in literature (Wei *et al.* 2018, Wei *et al.* 2019), in which the shield tunnel is also assumed to be a series of short beams connected by springs. While the beam calculation results show that it is the largest in the middle of the foundation pit.

4.3 Comparison with an existing case from literature

The Dongfang Road Interchange project is located in

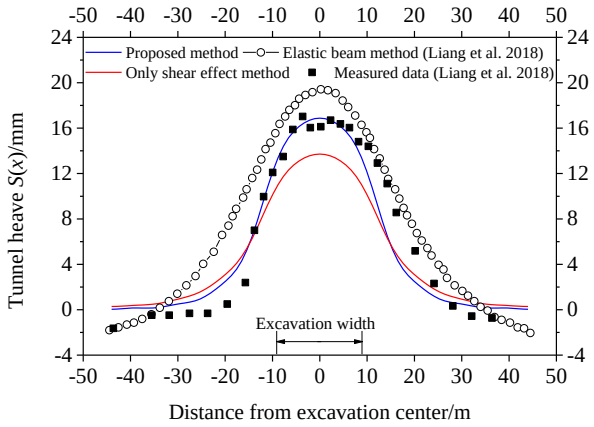

Fig. 12 Tunnel displacements with different methods

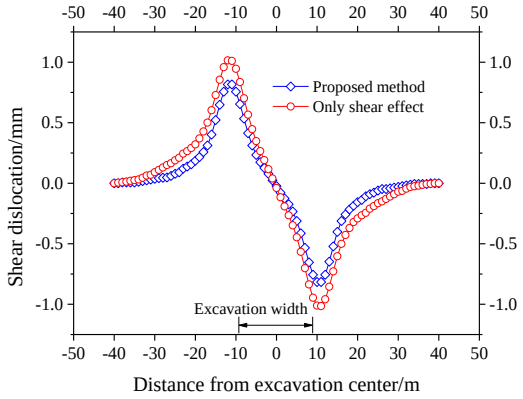

(a) Shear dislocation

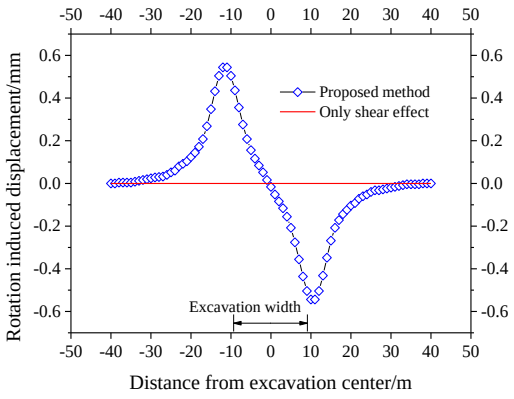

(b) Rotation induced displacement

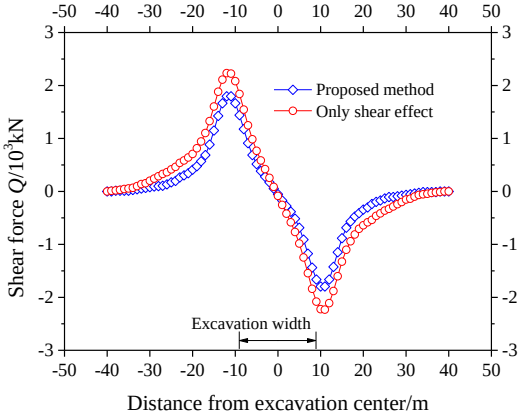

(c) Shear force

Fig. 13 Relative displacement and shear force distribution

Shanghai. The shape of the foundation pit is approximately a parallelogram with an average length of 26 m, a width of 18 m, and an angle of 66°(θ). The excavation depth is 6.5 m. The up-line tunnel of subway line 2 passes directly below the foundation pit, with an angle of 45°. The vault of the tunnel is 2.76 m away from the foundation pit floor. The outer diameter of the tunnel is 6.2 m and the buried depth is 12.36 m. The spatial relationship between the excavation and the tunnel is shown in Fig. 11, and the geological conditions can be found in Liang *et al.* (2018). According to Liang *et al.* (2018), the soil elastic modulus is taken as 20 MPa, the bending stiffness is 7.8×10^7 kN•m^2. According to the Appendix, the shear stiffness, the tensile stiffness and the compressive stiffness are taken as 2.47×10^6 kN/m, 1.73×10^5 kN/m and 1.79×10^8 kN/m.

The proposed method was used to predict the displacement of the existing tunnel caused by excavation. In the previous analysis method, a shield tunnel is regarded as an elastic beam (elastic beam method) or a series of short beams connected by shear springs between lining rings (shear effect method) which can consider the shear effect of the tunnel. Fig.12 shows the vertical displacement of the tunnel caused by the excavation of the foundation pit calculated by the three methods, in comparison with the

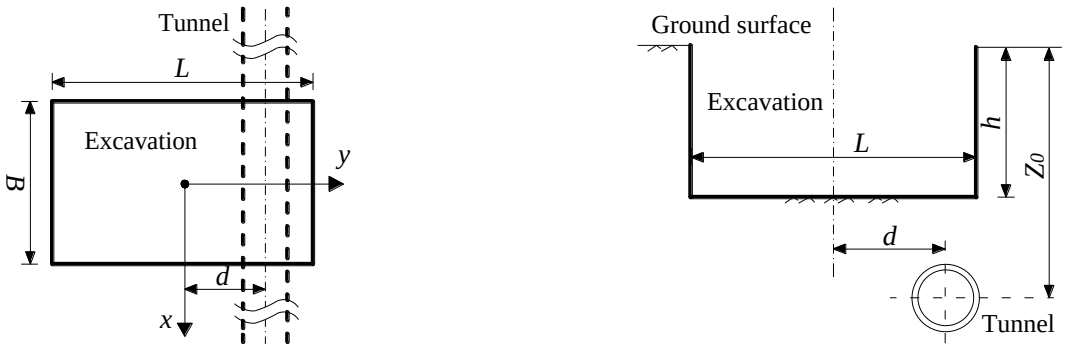

(a) Plan view (b) Sectional view

Fig. 14 Relative position between excavation and tunnel

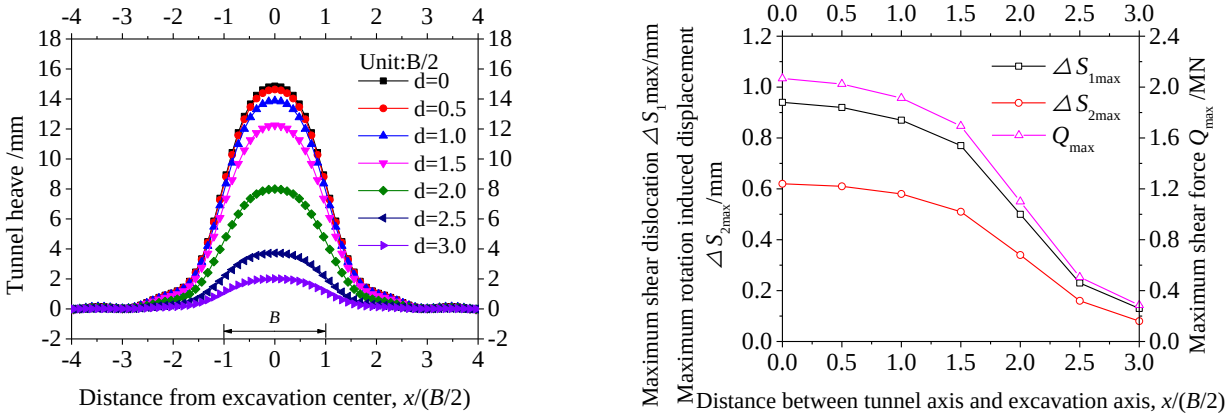

(a) Tunnel heave along tunnel longitudinal direction (b) Relative displacement and inter force

Fig. 15 Tunnel deformation and inter force with different excavation-tunnel distance

field measured data. It can be seen that the calculation results of our new method are basically consistent with the distribution of the measured data in the field, although there are some differences in the values. The displacement predicted by the elastic beam method is also in consistent with the measured data, although the maximum heave and the width of the curve trough are slightly overestimated. Compared the method in this paper, the results predicted by the shear effect method underestimate the heave of the tunnel, which is mainly because our new method not only considers the shear effect between the tunnel lining rings, but also considers the rotation effect of the lining ring, while the shear effect method only considers the shear effect. Compared with the measured data, the results obtained by the proposed method and the elastic beam method are in good agreement and the proposed method has a higher degree of agreement. This shows that our new method is suitable for the prediction of deformation of existing tunnel caused by excavation of foundation pit.

Fig. 13 shows the shear dislocation, the rotational displacement and the shear force Q calculated by our new method and the shear effect method. It can be seen from Fig. 13(a) that the shear dislocation is symmetric about the origin and reaches the maximum value at a location not far from the origin. In Comparison, the shear effect method gives larger shear dislocation. This is mainly because the shear effect method only considers the shear effect thus only the shear force to resist the unloading caused by the excavation of the foundation pit, thus causing the overestimation of the shear dislocation. This also explains why the bolts' shear force calculated by the shear effect method in Fig. 13(c) is larger. Fig. 13(b) shows the variation of rotation induced displacement along the tunnel longitudinal direction. The trend of the curve is similar to the shear dislocation. The shear effect method cannot provide rotation induced displacement because the method cannot consider the rotation effect.

It can be seen that the maximum shear force appears near the location of the retaining wall. And the maximum relative displacement of the tunnel also appears in the same location. Therefore, this part of the tunnel is more vulnerable to damage, and effective protection measures should be taken to protect the segment lining from shear effect.

5. Parametric analyses

In this section, based on a simple hypothetical example, the effects of various parameters (i.e. relative position of the tunnel and the excavation, shear stiffness, tensile stiffness, and rotation coefficient) on the tunnel are analyzed. The relative position of the tunnel and the excavation is shown in Fig. 14. The excavation pit length L, width B, and depth h are 40 m, 20 m and 10 m, respectively. The tunnel is perpendicular to the long side of the foundation pit, and the

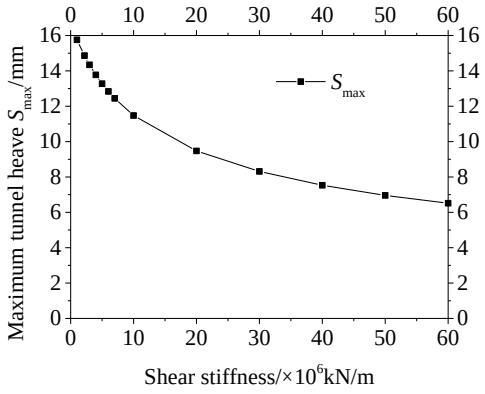

(a) tunnel heave

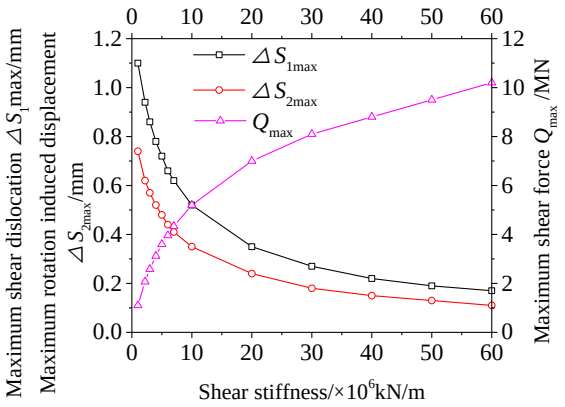

(b) Relative displacement and inter force

Fig. 16 Sensitivity of deformation to shear stiffness

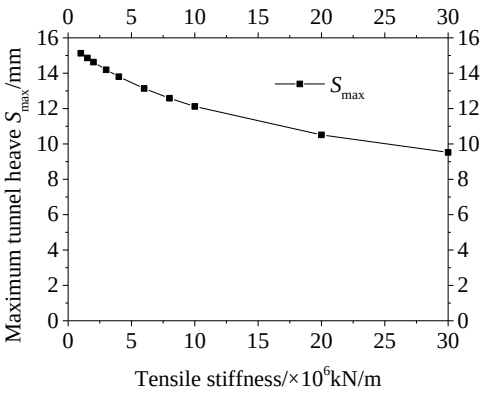

(a) Tunnel heave

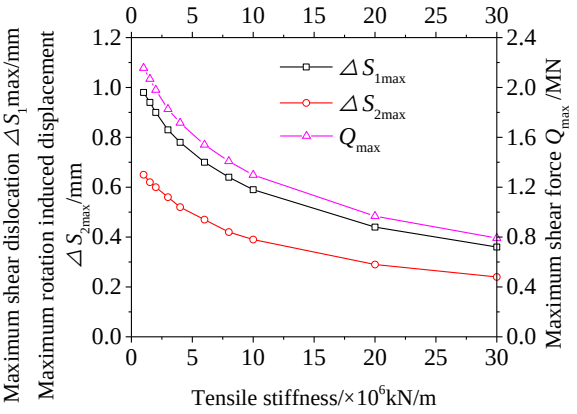

(b) Relative displacement and inter force

Fig. 17 Sensitivity of deformation to tensile stiffness

buried depth Z_0 is 15 m. The shear stiffness, the tensile stiffness and the compressive stiffness are taken as 2.2×10^6 kN/m, 1.52×10^5 kN/m and 1.79×10^8 kN/m. The Young's modulus of the ground is 15 MPa, and the average soil unit weight is 18 kN/m. The Poisson's ratio is 0.3.

5.1 Influence of the excavation-tunnel relative positions

Fig. 15(a) shows the distribution of the tunnel heave along the tunnel longitudinal direction. Normalize the distance in $B/2$. It can be seen that the tunnel heave decreases with the increase of the unit distance $x/(B/2)$; similarly, the tunnel heave decreases as the distance between the tunnel axis and the excavation axis d increases. When $d = 0$, the tunnel heave reaches the maximum value. When $0 < d < 1.5$ ($B/2$), the tunnel heave decreases slowly, however when $d > 1.5$ ($B/2$), the tunnel heave decreases rapidly. Liang *et al.* (2017) gave similar results. Fig. 15(b) shows the variation of shear dislocation, rotational displacement and shear force with the change of the distance between the tunnel and the excavation d. The maximum shear dislocation decreases with the increase of relative distance d. When $0 < d < 1.5$ ($B/2$), the reduction rate is slow and after $d > 1.5$ ($B/2$), the reduction rate increases rapidly. The trend of shear force and rotation displacement is the same as shear dislocation. It can be seen that increasing the relative distance between the tunnel and the excavation can effectively reduce the tunnel deformation caused by the excavation. And when excavating the foundation pit above the existing tunnel, the safety of the tunnel below should be paid attention to.

5.2 Influence of shear stiffness

Fig. 16(a) shows the variation of maximum tunnel heave with the change of shear stiffness. With the increase of shear stiffness, the maximum heave of the tunnel decreases. This is mainly because the increase of shear stiffness makes it difficult for the tunnel to shear dislocated. For the same additional load, the calculated heave is smaller. Similarly, as the shear stiffness increases, the maximum shear dislocation and the maximum rotation induced displacement also decrease, but the maximum shear force increases, as illustrated in Fig. 16(b). It can be seen that the increase in shear stiffness makes the connection between the lining rings of the tunnel more stable, and the deformation caused by the additional load can be resisted by a larger shear force. However, this does not mean that increasing shear stiffness is the most effective way to reduce tunnel deformation. Because when the shear stiffness increases from 1×10^6 kN/m to 1×10^7 kN/m, the tunnel heave and the

relative displacement between the rings decrease obviously. By further improving the shear stiffness, it is still observed that the deformation decreases, but the rate is slow. In addition, with the increase of shear stiffness, the shear force increases all the time. Therefore, the shear stiffness can be increased appropriately to alleviate the tunnel deformation, but it should not be relied upon only.

5.3 Influence of tensile stiffness

Fig. 17 shows the variation of tunnel heave and inter-ring displacement with tensile stiffness. The tensile stiffness and compressive stiffness have some effect on the rotation of the tunnel lining ring. Since the compression stiffness of the lining ring is much larger than the tensile stiffness of the bolt, the tensile stiffness of the bolt has more pronounced effects on tunnel deformation. Therefore, we only conduct parametric analysis on tensile stiffness.

Fig. 17(a) present sensitivity of tunnel heave to tensile stiffness. With the increase of tensile stiffness, the maximum heave the tunnel decrease. Fig. 17(b) shows the variations of the shear dislocation, rotation induced displacement and shear force with tensile stiffness. As the tensile stiffness increases, the rotation induced displacement decreases, which indicates that the rotation of the lining ring is restrained by the larger tensile stiffness. The shear dislocation also decreases with increasing tensile stiffness and the shear force also shows a weakening trend. Like shear stiffness, the increase of tensile stiffness weakens the heave of tunnel and the inter-ring displacement in different degrees. When the tensile stiffness increases from 1×10^5 kN/m to 1×10^6 kN/m, the tunnel heave, relative displacement and shear force decrease obviously. By further improving the tensile stiffness, the rate of reduction is small. Therefore, appropriately increasing the tensile stiffness can alleviate the tunnel deformation, but it will not work when the tensile stiffness is large enough.

6. Conclusions

Due to the presence of joints of shield tunnel, the overall tunnel stiffness is significantly reduced. The excavation of adjacent deep foundation pit has adverse impacts on the existing tunnels. In order to ensure the safety and integrity of tunnel structures, it is necessary to study the interaction between deep excavation and tunnel. In this work a simplified analytical method is proposed to calculate the deformational response of an existing tunnel to a deep excavation. In the calculation, the existing tunnel is assumed to be buried in elastic and homogeneous soil and always connected with the soil. This method first estimates the additional force at the existing tunnel level induced by the excavation of deep foundation pit, and then uses the energy method to solve the deformation of the tunnel. The following conclusions can be drawn:

• In this work, a simplified semi-analytical method for evaluating the heave of underlying tunnel induced by new excavation is presented. The new model assumes the tunnel can be modeled by a series of short beams connected by the shear springs, tensile springs and compressive springs. The model can capture the shear effect between the linings and the rotation effect of the lining ring, making it possible to more reliably describe and predict the actual mechanical behaviors and the deformation of shield tunnels.

• Compared with the existing beam methods, the method proposed in this work can consider the bolt connection between the lining rings and evaluate the tunnel deformation that consists of contributions of shear dislocation and lining ring rotation. The effectiveness of the proposed method is validated through two case studies and numerical analysis. The calculation results of the proposed model are consistent with the field measured data. This method can quickly predict the displacement of tunnel so may be adopted in the pre-assessment and optimization of construction plans.

• Through parametric study, the effects of the excavation-tunnel relative positions, the shear stiffness between the lining rings, the tensile stiffness of the bolts, and the rotation effect coefficient on the deformation behavior of the existing tunnel are experimented. As the shear or tensile stiffness increases, the tunnel heave and inter-ring displacement decreases. This shows that an appropriate increase in stiffness helps retain the integrity and stability of the tunnel.

• It should be noted that the embossed groove between the lining rings is not considered in the calculation of the shear stiffness. The shear stiffness of the bolts is approximately represented by the shear stiffness between the lining rings. This simplification will be further investigated in our future work.

Acknowledgments

This study is mainly supported by “National Key Research and Development Program of the 13th Five-Year Plan of China [sub-project No. 2016YFC080250504]”.

Data availability statement

The date used to support the findings of this study are available from the corresponding author upon request.

References

Basile, F. (2014), “Effects of tunnelling on pile foundations”, *Soils Found.*, **54**(3), 280-295. https://doi.org/10.1016/j.sandf.2014.04.004.

Bousbia, N. and Messast, S. (2015), “Numerical modeling of two parallel tunnels interaction using three-dimensional Finite Elements Method”, *Geomech. Eng.*, **9**(6), 775-791. https://doi.org/10.12989/gae.2015.9.6.775.

Cheng, W.C., Ni, J.C. and Shen, S.L. (2017), “Experimental and analytical modeling of shield segment under cyclic loading”, *Int. J. Geomech.*, **17**(6), 04016146. https://doi.org/10.1061/(ASCE)GM.1943-5622.0000810.

Do, N.A., Dias, D. and Oreste, P. (2018), “Numerical investigation of segmental tunnel linings-comparison between the hyperstatic reaction method and a 3D numerical model”, *Geomech. Eng.*, **14**(3), 293-299. https://doi.org/10.12989/gae.2018.14.3.293.

Han, X., Liu, C.W. and Standing, J.R. (2012), “Structural

settlement of existing tunnel caused by new tunnel excavated underneath", *China Civ. Eng. J.*, **45**(1),134-141 (In Chinese). http://doi.org/10.15951/j.tmgcxb.2012.01.008.

Huang, X., Schweiger, H.F. and Huang, H. (2013), "Influence of deep excavations on nearby existing tunnels", *Int. J. Geomech.*, **13**(2), 170-180. https://doi.org/10.1061/(ASCE)GM.1943-5622.0000188.

Li, P., Du, S.J., Shen, S.L., Wang, Y.H. and Zhao, H.H. (2016), "Timoshenko beam solution for the response of existing tunnels because of tunneling underneath", *Int. J. Numer. Anal. Met.*, **40**(5), 766-784. https://doi.org/10.1002/nag.2426.

Liang, R., Xia, T.D., Huang, M.S. and Lin, C.G. (2017), "Simplified analytical method for evaluating the effects of adjacent excavation on shield tunnel considering the shearing effect", *Comput. Geotech.*, **81**, 167-187. https://doi.org/10.1016/j.compgeo.2016.08.017.

Liang, R.Z., Wu, W.B., Yu, F., Jiang, G.S. and Liu, J.W. (2018), "Simplified method for evaluating shield tunnel deformation due to adjacent excavation", *Tunn. Undergr. Sp. Tech.*, **61**, 104-121. https://doi.org/10.1016/j.tust.2017.08.010.

Liu, B., Yu, Z.W., Han, Y.H., Wang, Z.L., Zhang, R.H. and Wang, S.J. (2020), "Analytical solution for the response of an existing tunnel induced by above-crossing shield tunneling", *Comput. Geotech.*, **124**(8), 103624.

Liu, H.L., Li, P. and Liu, J.Y. (2011), "Numerical investigation of underlying tunnel heave during a new tunnel construction", *Tunn. Undergr. Sp. Tech.*, **26**(2), 276-283. https://doi.org/10.1016/j.tust.2010.10.002

Liu, X., Fang, Q., Zhang, D.L. and Wang, Z.J. (2019), "Behaviour of existing tunnel due to new tunnel construction below", *Comput. Geotech.*, **110**, 71-81. https://doi.org/10.1016/j.compgeo.2019.02.013.

Marshall, A.M., Klar, A. and Mair, R.J. (2010), "Tunnelling beneath buried pipes: View of soil strain and its effect on pipeline behavior", *J. Geotech. Geoenviron. Eng.*, **136**(12), 1664-1672. https://doi.org/10.1061/(ASCE)GT.1943-5606.0000390.

Mindlin, R.D. (1936), "Force at a point in the interior of a semi-infinite solid", *J. Appl. Phys.*, **7**(5), 195-202. https://doi.org/10.1063/1.1745385.

Nam, K., Kim, J., Kwak, D., Rehman, H. and Yoo, H.Y. (2020), "Structure damage estimation due to tunnel excavation based on indoor model test", *Geomech. Eng.*, **21**(2), 95-102. https://doi.org/10.12989/gae.2020.21.2.095.

Ng, C.W., Shi, J. and Hong, Y. (2013), "Three-dimensional centrifuge modelling of basement excavation effects on an existing tunnel in dry sand", *Can. Geotech. J.*, **50**(8), 874-888. http://doi.org/10.1139/cgj-2012-0423.

Nooraddin, N. and Mohammad, F.M. (2016), "Analysis of stress distribution around tunnels by hybridized FSM and DDM considering the influences of joints parameters", *Geomech. Eng.*, **11**(2), 269-288. https://doi.org/10.12989/gae.2016.11.2.269.

Poulos, H.G. and Davis, E.H. (1980), *Pile Foundation Analysis and Design*, Wiley, New York, U.S.A.

Shi, J., Ng, C.W.W. and Chen, Y. (2015), "Three-dimensional numerical parametric study of the influence of basement excavation on existing tunnel", *Comput. Geotech.*, **63**, 146-158. http://doi.org/10.1016/j.compgeo.2014.09.002.

Talmon, A.M. and Bezuijen, A. (2013), "Calculation of longitudinal bending moment and shear force for Shanghai Yangtze river tunnel: Application of lessons from Dutch research", *Tunn. Undergr. Sp. Tech.*, **35**, 161-171. https://doi.org/10.1016/j.tust.2013.01.001.

Tanahashi, H. (2004), "Formulas for an infinitely long Bernoulli-Euler beam on the Pasternak model", *Soils Found.*, **44**(5), 109-18. http://doi.org/10.3208/sandf.44.5.109.

Vorster, T.E.B., Klar, A., Soga, K. and Mair, R.J. (2005), "Estimating the effects of tunnelling on existing pipelines", *J. Geotech. Geoenviron. Eng.*, **131**(11), 1399-1410. https://doi.org/10.1061/(ASCE)1090-0241(2005)131:11(1399).

Wang, L., Zou, J.F., Yang, T. and Wang, F. (2019), "Elastic solutions for shallow tunnels excavated under non-axisymmetric displacement boundary conditions on a vertical surface", *Geomech. Eng.*, **19**(3), 201-215. https://doi.org/10.12989/gae.2019.19.3.201.

Wei, G., Hong, W.Q., Wei, X.J., Zhang, X.H. and Luo, J.W. (2019), "Calculation of rigid body rotation and shearing dislocation deformation of adjacent shield tunnels due to excavation of foundation pits", *Chin. J. Geotech. Eng.*, **41**(7), 1251-1259 (In Chinese).

Wei, X.J., Hong, W.Q., Wei, G. and Yu, G.H. (2018), "Rotation and shearing dislocation deformation of subway tunnels due to adjacent ground stack load", *Chin. J. Rock Mech. Eng.*, **37**(5), 1281-1289 (In Chinese).

Winkler, E., (1867), *Die Lehre von der Elastizität und Festigkeit [The Theory of Elasticity and Stiffness]*, H. Dominicus Prague, Czech Republic (in German).

Wu, H.N., Shen, S.L., Liao, S.M. and Yin, Z.Y. (2015), "Longitudinal structural modelling of shield tunnels considering shearing dislocation between segmental rings", *Tunn. Undergr. Sp. Tech.*, **50**, 317-323. https://doi.org/10.1016/j.tust.2015.08.001.

Zhang, D.M., Huang, Z.K., Li, Z.L., Zong, X. and Zhang, D.M. (2019), "Analytical solution for the response of an existing tunnel to a new tunnel excavation underneath", *Comput. Geotech.*, **108**, 197-211. https://doi.org/10.1016/j.compgeo.2018.12.026

Zhang, J.F., Chen, J.J., Wang, J.H. and Zhu, Y.F. (2013), "Prediction of tunnel displacement induced by adjacent excavation in soft soil", *Tunn. Undergr. Sp. Tech.*, **36**, 24-33. https://doi.org/10.1016/j.tust.2013.01.011.

Zhang, Z., Zhang, M. and Zhao, Q. (2015), "A simplified analysis for deformation behavior of buried pipelines considering disturbance effects of underground excavation in soft clays", *Arab. J. Geosci.*, **8**(10), 1-15. https://doi.org/10.1007/s12517-014-1773-4

Zhang, Z.G. and Huang, M.S. (2014), "Geotechnical influence on existing subway tunnels induced by multiline tunneling in Shanghai soft soil", *Comput. Geotech.*, **56**, 121-132. https://doi.org/10.1016/j.compgeo.2013.11.008.

Zhang, Z.G., Zhao, Q. H. and Zhang, M.X. (2016), "Deformation analyses during subway shield excavation considering stiffness influences of underground structures", *Geomech Eng*, **11**(1), 117-139. https://doi.org/10.12989/gae.2016.11.1.117.

Zheng, G., Du, Y.M., Cheng, X.S., Diao, Y., Deng, X. and Wang, F.J. (2017), "Characteristics and prediction methods for tunnel deformations induced by excavations", *Geomech. Eng.*, **12**(3), 361-397. https://doi.org/10.12989/gae.2017.12.3.361.

Zhou, N. and Yuan, Y. (2009), "Correlation of cross-river shield tunnel between longitudinal deformation curvature and segment Leakage", *Journal of Tongji University (Natural Science)*, **37**(11), 1446-1451,1501. (in Chinese).

CC

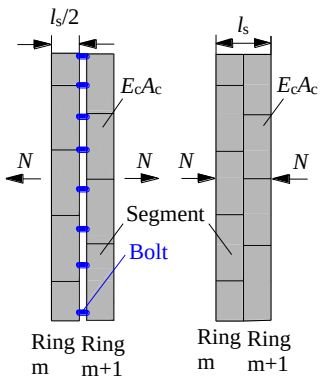

Fig. 18 Calculation of the tensile and compression stiffness

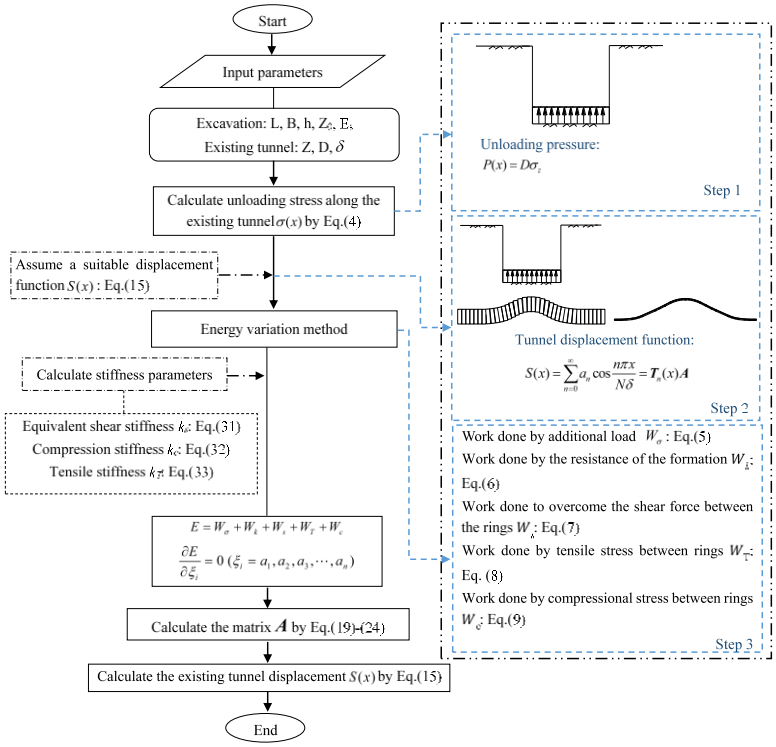

Fig. 19 Flow chart of implementing the method developed in this work

Appendix

A.1 Equivalent shear stiffness

Wu *et al.* (2015) proposed a formula for calculating the equivalent shear stiffness of shield tunnels. In their work the unit shear displacement u is composed of the segment shear deformation u_j and the bolt shear deformation u_s:

$$u = u_j + u_s \tag{26}$$

u, u_j, u_s are expressed as:

$$u = l_s \tan\frac{Q}{k_s} \tag{27}$$

$$u_j = l_b \tan\frac{Q}{n\kappa_b G_b A_b} \tag{28}$$

$$u_s = (l_s - l_b)\tan\frac{Q}{\kappa_c G_c A_c} \tag{29}$$

where κ_b and κ_c are the shear coefficients of the bolt and segment ring, respectively. For circular section bolts, κ_b = 0.9; for annular tunnel segment rings, κ_c = 0.5. G_b and G_c are the bolt shear modulus and the segmental ring shear modulus, respectively.

G_b and G_c are expressed as:

$$G_b = \frac{E_b}{2(1+\nu_b)}, G_c = \frac{E_c}{2(1+\nu_c)} \tag{30}$$

Among them, ν_b and ν_c are Poisson's ratios of bolts and segments respectively.

From Eqs. (24)-(27), we can obtain:

$$k_s = \xi l_s \left(\frac{l_b}{n\kappa_b G_b A_b} + \frac{l_s - l_b}{\kappa_c G_c A_c}\right)^{-1} \tag{31}$$

A.2 Tensile and compressive stiffness

We take l_s in Fig. 18 between the center lines of the two segment rings as a calculation unit. When the lining ring is under pressure, only the segment ring is compressed and the bolt does not deform; while the lining ring is under tension, the segment and the bolts are simultaneously stretched.

The tensile and compressive stiffness are as follows:

$$k_c = \frac{E_c A_c}{l_s} \tag{32}$$

$$k_T = E_c A_c \left(1 + \frac{E_c A_c}{l_s k_b l_b / \lambda I_b} \right)^{-1} \tag{33}$$

I_b is the moment of inertia; k_b is the elastic rigidity of the bolt; λ is the influence coefficient of the bolt between lining rings, according to Zhou and Yuan (2009), it may be set to 0.6225. E_c, A_c, are as defined above.

A.3 Flow chart